The Journal of Chemical Physics

Dissipative particle dynamics with energy conservation: Isoenergetic integration and transport properties

Cite as: J. Chem. Phys. **152**, 064112 (2020); https://doi.org/10.1063/1.5119778
Submitted: 12 July 2019 . Accepted: 28 January 2020 . Published Online: 13 February 2020

Fatemeh A. Soleymani, Marisol Ripoll, Gerhard Gompper, and Dmitry A. Fedosov

The Journal of Chemical Physics ARTICLE scitation.org/journal/jcp

Dissipative particle dynamics with energy conservation: Isoenergetic integration and transport properties

Cite as: J. Chem. Phys. 152, 064112 (2020); doi: 10.1063/1.5119778
Submitted: 12 July 2019 • Accepted: 28 January 2020 •
Published Online: 13 February 2020

Fatemeh A. Soleymani, Marisol Ripoll,[a] Gerhard Gompper,[b] and Dmitry A. Fedosov[c]

AFFILIATIONS

Theoretical Soft Matter and Biophysics, Institute of Complex Systems and Institute for Advanced Simulation, Forschungszentrum Jülich, 52425 Jülich, Germany

[a]Electronic mail: m.ripoll@fz-juelich.de
[b]Electronic mail: g.gompper@fz-juelich.de
[c]Author to whom correspondence should be addressed: d.fedosov@fz-juelich.de

ABSTRACT

Simulations of nano- to micro-meter scale fluidic systems under thermal gradients require consistent mesoscopic methods accounting for both hydrodynamic interactions and proper transport of energy. One such method is dissipative particle dynamics with energy conservation (DPDE), which has been used for various fluid systems with non-uniform temperature distributions. We propose an easily parallelizable modification of the velocity-Verlet algorithm based on local energy redistribution for each DPDE particle such that the total energy in a simulated system is conserved up to machine precision. Furthermore, transport properties of a DPDE fluid are analyzed in detail. In particular, an analytical approximation for the thermal conductivity coefficient is derived, which allows its *a priori* estimation for a given parameter set. Finally, we provide approximate expressions for the dimensionless Prandtl and Schmidt numbers, which characterize fluid transport properties and can be adjusted independently by a proper selection of model parameters. In conclusion, our results strengthen the DPDE method as a very robust approach for the investigation of mesoscopic systems with temperature inhomogeneities.

I. INTRODUCTION

Simulations of mesoscopically structured systems, ranging from supra-molecular assemblies and artificial self-propelled microswimmers to the flow of biological cell suspensions in complex environments, have become important in studies of a broad variety of biophysical, biomedical, and engineering applications.[1–4] This has driven a rapid development of mesoscopic simulation methods employed to advance our understanding of such systems.[5,6] Mesoscopic methods usually neglect molecular details but retain features of suspended particles, such as deformability, inter-particle forces, or thermal fluctuations. Examples of mesoscopic methods are the lattice Boltzmann method (LBM),[7–9] multiparticle collision dynamics (MPC),[6,10–12] and dissipative particle dynamics (DPD).[13–15]

Studies of many interesting phenomena require modeling of non-isothermal environments, where temperature gradients are significant, and transport of energy might be relevant. Examples include heat transfer,[16] thermodiffusion in binary mixtures,[17–20] and colloidal thermophoresis.[21–25] Such problems generally rely on simulation methods which are able to represent the system in a micro-canonical ensemble where energy is exactly conserved. Various non-isothermal systems have been modeled using molecular dynamics,[19,26] thermal LBM,[27,28] MPC,[29–31] and an energy-conserving version of the Monte Carlo method.[32] The original DPD method[13,14] is isothermal and has been extended to account for energy conservation (DPDE).[33,34] DPDE has successfully been applied to simulate a number of thermal gradient problems, such as natural[35] and forced convection,[36] temperature-dependent fluid properties,[37] droplet flows,[38] and thermophoretic Janus colloids.[23]

Several algorithms have been employed in DPDE, including velocity-Verlet (VV)-based schemes[39–42] and Shardlow-splitting (SS)-based algorithms.[37,41–46] One of the problems of many integration schemes is that they yield a significant net energy drift, rendering long-time integration difficult. In particular, VV-based schemes[41,42] are prone to strong energy-drift problems, which can be reduced by decreasing the integration time step. However,

this makes the method less attractive as it becomes more CPU-time consuming. SS-based algorithms[37,41–46] exhibit much less severe energy-drift problems and, therefore, allow larger integration time steps. Nevertheless, SS schemes are generally more expensive computationally than simple VV algorithms and are difficult to parallelize and to utilize multithreading.[42–45] Another problem of many algorithms is their stability for large time steps or low heat capacities, which generally occurs due to a possible appearance of negative internal energies. This drawback has recently been eliminated by introducing a Metropolis–Hastings procedure for stochastic interactions within the SS algorithm.[44,45] Furthermore, it is not fully clear whether the DPDE method can faithfully represent important features (e.g., thermal diffusivity and momentum transport) of real fluids as the transport properties of a DPDE fluid are not straightforwardly predetermined.

In this paper, we suggest a modification of the well-known VV algorithm by local energy redistribution (LER), which results in the conservation of total energy of a simulated system up to the order of machine precision and completely eliminates energy drift. Within the LER algorithm, changes in kinetic and potential energies are counterbalanced by the internal energy at the level of each DPDE particle such that the local energy is conserved with a good accuracy, while the total energy is conserved exactly. We investigate the performance of the LER algorithm for several choices of conservative interactions between particles, which affect the fluid compressibility. Furthermore, an analytical approximation of the overall thermal conductivity κ of a DPDE fluid is derived, which allows its direct estimation for selected simulation parameters. The thermal conductivity is governed by two contributions: (i) direct heat conduction and (ii) diffusive heat transport, whose relative ratio can be estimated from the analytical approximation of κ. Finally, we study the dimensionless Prandtl and Schmidt numbers characterizing fluid transport properties and show that they can independently be adjusted to match those of real fluids.

The paper is organized as follows. Section II provides details about the DPDE method and the LER integration algorithm, with the details given in the Appendix. In Sec. III, the DPDE method is validated and its performance is studied under thermal gradient conditions. In Sec. III, we also derive the analytical approximation of the fluid thermal conductivity coefficient and discuss transport properties of simulated liquids in comparison with real fluids.

II. METHODS AND MODELS

A. DPDE governing equations

In the same spirit as in the isothermal DPD method,[13,14,47] DPDE particles are mesoscopic entities, which represent small fluid volumes containing numerous atoms or molecules. The N constituent particles are characterized by their positions $\mathbf{r}_i$ and velocities $\mathbf{v}_i$. Furthermore, each of the DPDE particles is characterized by an additional variable accounting for the internal energy ϵ_i of the small fluid volume. This energy is connected to an internal temperature $T(\epsilon)$ via an entropy function $S(\epsilon)$ or, equivalently, the density of internal states, as $\partial S(\epsilon)/\partial \epsilon = 1/T(\epsilon)$, which corresponds to the related thermodynamic force.[48] A simple choice for the entropy function is that of an ideal solid, i.e., $S(\epsilon) = c_v \ln(\epsilon) + \text{const}$, where c_v is the heat capacity at constant volume. This choice results in a straightforward linear relation between internal energy and temperature as $\epsilon_i = c_v T_i$.[33,34,49,50] The dimensionless heat capacity c_v/k_B is generally a large number since it is a measure of the size of a DPDE particle which characterizes the number of internal degrees of freedom for this particle.

Time evolution of particle characteristics (i.e., position, velocity, and internal energy) is governed by Newton's equation of motion and heat equation,

$$\frac{\mathrm{d}\mathbf{r}_i}{\mathrm{d}t} = \mathbf{v}_i, \quad \frac{\mathrm{d}\mathbf{v}_i}{\mathrm{d}t} = \frac{1}{m_i}\mathbf{F}_i, \quad c_v \frac{\mathrm{d}T_i}{\mathrm{d}t} = q_i. \tag{1}$$

Here, m_i is the particle mass, $\mathbf{F}_i$ is the total force, and q_i is the total heat rate.

The force $\mathbf{F}_i$ on particle i is a sum of three pairwise interactions with neighboring particles j given by

$$\mathbf{F}_i = \sum_{j\neq i}\left(\mathbf{F}_{ij}^C + \mathbf{F}_{ij}^D + \mathbf{F}_{ij}^R\right). \tag{2}$$

The three contributions correspond to the conservative, dissipative, and random forces which take the form

$$\begin{aligned}\mathbf{F}_{ij}^C &= a_{ij}\omega^C(r_{ij})\hat{\mathbf{r}}_{ij},\\ \mathbf{F}_{ij}^D &= -\gamma_{ij}\omega^D(r_{ij})(\mathbf{v}_{ij}\cdot\hat{\mathbf{r}}_{ij})\hat{\mathbf{r}}_{ij},\\ \mathbf{F}_{ij}^R &= \sigma_{ij}\omega^R(r_{ij})\xi_{ij}\Delta t^{-1/2}\hat{\mathbf{r}}_{ij}.\end{aligned} \tag{3}$$

Here, $\mathbf{r}_{ij} = \mathbf{r}_i - \mathbf{r}_j$, $\mathbf{v}_{ij} = \mathbf{v}_i - \mathbf{v}_j$, $r_{ij} = |\mathbf{r}_{ij}|$, $\hat{\mathbf{r}}_{ij} = \mathbf{r}_{ij}/r_{ij}$, and Δt is the integration time step. The conservative-force coefficient a_{ij} controls fluid compressibility. The coefficients γ_{ij} and σ_{ij} represent friction and noise amplitudes that are connected to each other through the fluctuation-dissipation relation[33,34,51] as

$$\gamma_{ij} = \frac{\sigma_{ij}^2}{4k_B}\left(\frac{1}{T_i} + \frac{1}{T_j}\right) \tag{4}$$

with the Boltzmann constant k_B. The random force is determined by ξ_{ij}, a symmetric Gaussian random variable (i.e., $\xi_{ij} = \xi_{ji}$) with zero mean and unit variance. Generally, σ_{ij} is selected as a constant and γ_{ij} is calculated according to Eq. (4). The interaction strengths in Eq. (3) are further controlled by the weight functions which are most commonly chosen as

$$\omega(r_{ij}) = \begin{cases}\left(1 - \dfrac{r_{ij}}{r_c}\right)^{2s}, & r_{ij} \le r_c,\\ 0, & r_{ij} > r_c,\end{cases} \tag{5}$$

where r_c is the cutoff radius and $s > 0$ is an exponent controlling the interaction strength. While the dissipative and the random functions are linked via the fluctuation-dissipation theorem as $\omega^D = \left(\omega^R\right)^2 = \omega$,[14] the choice of the conservative function ω^C is independent.

B. Heat conduction

The time evolution of the internal temperature (or the corresponding internal energy) is governed by the third equality in Eq. (1). The amount of heat that each particle receives (or loses) from its close neighbors per unit time can be expressed as

$$q_i = \sum_{j\neq i}\left(q_{ij}^{HC} + q_{ij}^{VH}\right), \tag{6}$$

where q_{ij}^{HC} corresponds to *heat conduction* and q_{ij}^{VH} corresponds to *viscous heating*.

DPDE particles are characterized by an intrinsic temperature such that every pair of particles is expected to exchange some heat by conduction, a process which has to be explicitly modeled. A commonly employed heat-conduction term[33,34] is proportional to the difference in thermodynamic forces (i.e., in the inverse temperatures) as

$$q_{ij}^{HC} = \kappa_{ij}\omega^H(r_{ij})\left(\frac{1}{T_i} - \frac{1}{T_j}\right) + \alpha_{ij}\zeta_{ij}\left[\omega^H(r_{ij})/\Delta t\right]^{1/2}, \tag{7}$$

where κ_{ij} and α_{ij} are heat-conduction coefficients of the deterministic and random terms, respectively. To guarantee energy conservation, each term in Eq. (7) needs to be antisymmetric under particle interchange. The deterministic term is antisymmetric by construction, and the fluctuating factor ζ_{ij} is defined as an antisymmetric Gaussian variable with zero mean and unit variance such that $\zeta_{ij} = -\zeta_{ji}$. Note that ζ_{ij} is completely uncorrelated with ξ_{ij}. Detailed balance imposes the relation between the deterministic and fluctuating terms. Thus, the heat-conduction coefficients are connected by the fluctuation-dissipation relation $\alpha_{ij}^2 = 2k_B\kappa_{ij}$, where $\kappa_{ij} = \kappa_0 c_v^2(T_i + T_j)^2/4k_B$ with the constant nominal strength κ_0. The weight function ω^H can generally be chosen independent of the other weight functions, but for simplicity, the standard selection is $\omega^H = \omega^D$.

Thermodynamic consistency of the q_{ij}^{HC} expression, with the existence of an $\mathcal{H}$-theorem and a proper equilibrium distribution, has been shown theoretically.[33,34,51] In particular, it has been shown that the equilibrium distribution function is proportional to the degeneracy factor $g(\epsilon_i) \equiv \exp[s(\epsilon_i)/k_B] \propto \epsilon_i^{c_v/k_B}$ or the number of internal states with energy ϵ_i. The single-particle equilibrium distribution in the canonical ensemble is then

$$\psi_{eq}(\epsilon_i) = \frac{1}{Z(\beta)}\epsilon_i^{c_v/k_B}\exp[-\beta\epsilon_i], \tag{8}$$

where $\beta = 1/k_BT$ is the inverse of the macroscopic temperature and $Z(\beta)$ is the normalization factor or the corresponding single-particle partition function. This distribution function was already tested in simulations.[49]

C. Viscous heating: Isoenergetic integration

The second contribution to the heat transport in Eq. (6) is the viscous-heating term $q_i^{VH} = \sum_{i\neq j} q_{ij}^{VH}$, which represents the work done by conservative and dissipative forces. Thus, it accounts for the variation in mechanical energy as $q_i^{VH} = \delta E_{mec,i} = \delta P_i + \delta K_i$, where P_i and K_i are the potential and kinetic energies whose changes can be calculated as

$$\begin{aligned}\delta P_i &= -\sum_{i\neq j}\mathbf{F}_{ij}^C\cdot\delta\mathbf{r}_{ij},\\ \delta K_i &= m\sum_i \mathbf{v}_i\cdot\mathrm{d}\mathbf{v}_i + m\sum_i \mathrm{d}\mathbf{v}_i\cdot\mathrm{d}\mathbf{v}_i.\end{aligned} \tag{9}$$

The second sum in the variation of kinetic energy is a consequence of the stochastic contribution. By considering the equation of motion (1) and the form of the DPD forces in Eq. (3), the change in mechanical energy can be expressed explicitly through the DPD force parameters.[33,34] In fact, such non-trivial expressions for q_i^{VH} are often integrated directly using various existing methods such as SS or Trotter schemes.[52–54] However, we do not use such an expression but calculate q_i^{VH} by a direct tracking of changes in the kinetic and potential energies for every particle at each time step; see the Appendix for details about the LER algorithm which is implemented by our group within the LAMMPS package.[55] In this way, the viscous-heating contribution is redistributed into the internal energy, which results in local energy conservation with a good accuracy, while the total energy of a simulated system is exactly conserved. This idea is similar to the VV scheme with energy reinjection.[42] Furthermore, a study[41] focused on the performance of different variants of the SS scheme has also mentioned a similar idea, but the energy redistribution has been implemented at the level of particle pairs in contrast to the single-particle level proposed here, and the contribution of potential energy was not considered. A further important advantage of the LER algorithm is that it allows much more efficient parallelization and multithreading than more sophisticated algorithms, such as SS or Trotter schemes,[42,43] making it a powerful candidate for applications.

D. Simulation setup and parameters

Simulation units are selected to be the particle mass $m = 1$, the length of the cutoff radius $r_c = 1$, and the unit of energy $k_BT_0 = 1$ with the reference temperature T_0. In this way, $\tau = r_c\sqrt{m/(k_BT_0)} = 1$ corresponds to the unit of time. The default average temperature and number density of fluid particles are set to $\tilde{T} = T_0$ and $\tilde{\rho} = 3/r_c^3$, respectively, unless specified otherwise. The DPDE forces employ $\omega^C = \omega$ with $s = 0.5$ as used commonly in DPD, $\sigma = 3k_BT_0\sqrt{\tau}/r_c$, and $\omega^D = \omega^H = \omega$ with $s = 0.25$ whose value has been shown to increase the fluid viscosity in comparison with a frequently used value of $s = 1$.[56,57] The specific heat is set to $c_v = 200\,k_B$, and the nominal strength of interparticle heat conductivity is $\kappa_0 = 0.001/\tau$.

The conservative-force coefficient a_{ij} is typically taken as a constant in DPDE, following a similar choice in the classical DPD method. When a constant a_{ij} is employed, the particle density shows to be nearly independent of temperature. To better represent fluid properties, it was suggested to consider a_{ij} with an explicit temperature dependence.[37,58] We consider three cases: (i) the ideal-gas equation of state case with $a_{ij}^C = 0$, (ii) the case with a constant coefficient $a_{ij}^C = a_0$, and (iii) the case with a temperature-dependent coefficient $a_{ij}^T = a_0(T_i + T_j)/2\tilde{T}$, for which the default constant parameter is taken to be $a_0 = 15k_BT_0/r_c$. Note that the temperature-dependent repulsion amplitude can be rationalized in terms of multi-body DPD[59,60] since temperature changes affect local particle density. Following the discussion in Refs. 15 and 61, the fact that the repulsion amplitude has a linear dependence on the internal temperature and is symmetric under particle interchange ensures the existence of a well-defined potential for this choice of conservative interactions.

The default choice for the conservative-force coefficient employed in simulations is a^T if not stated otherwise. A default time step corresponds to $\Delta t = 0.005\tau$. Simulations are performed with periodic boundary conditions in a domain with dimensions $L_x = 20r_c$, $L_y = L_z = 10r_c$. All other parameters will be specified in the text whenever necessary.

III. RESULTS

A. Homogeneous temperature

1. Total energy conservation

One of the main issues of the DPD method is the establishment of an efficient and consistent algorithm for the integration of the DPD equations, which has been and still is treated in a large number of related studies.[58,62–66] Although DPDE was proposed as an energy-conserving method, so far all investigations, in which the viscous-heating term q_{ij}^{VH} is calculated explicitly through the system parameters,[37,41–43,52,53,67] have reported different deviations from energy-conserving behavior for various time steps and integration schemes. For example, Homman *et al.*[42] reported an energy drift within a range $1–2 \times 10^{-5} k_B T_0$ for $\Delta t = 0.006\tau$ and a total integration time of 10τ, while Lísal *et al.*[41,43] found an energy drift on the order of 10^{-4}, even though the viscous heat rate was not explicitly calculated. Furthermore, Li *et al.*[37] demonstrated fluctuations in the total energy on the order of $10^{-3} k_B T_0$, even though no significant energy drift within the total integration time was detected.

As explained in Sec. II C, the LER algorithm adopted here is fundamentally different from those used previously since the variation of energy per particle is directly monitored and used for the calculation of the viscous-heating term, avoiding its approximation in terms of parameters such as the relative velocities or positions of all neighboring particles. We have verified the conservation of total energy for a range of time steps $\Delta t/\tau \in [0.005; 0.05]$ and for two system sizes: the one with default values and another one approximately ten times larger. Maximum error and fluctuations in the total energy are found to be on the order of $10^{-14} k_B T_0$, which demonstrates that the LER algorithm conserves the total energy by construction (see the Appendix), and therefore, the error in total energy is directly associated with the machine precision.

Note that in order to evaluate the total energy, the mechanical energy needs to be considered together with the internal energy U_I. The internal energy constitutes the dominant contribution to the total energy since $U_I \approx N c_v T_0$ and $c_v \gg k_B$, and the kinetic energy is $K \simeq 3 N k_B T_0/2$ (i.e., $U_I/K \simeq 2c_v/3\,k_B$), while our simulations show that the potential energy is $P \simeq 2K$ for the default conservative interactions.

2. Temperature definition

In the DPDE method, three temperatures can be defined which, for consistency, should be equivalent. The internal temperature T_I is computed by averaging over the internal particle temperatures $\langle T_i \rangle$; the kinetic temperature T_K is calculated by averaging the kinetic energy of all particles as $\langle m_i v_i^2/3 \rangle$, and they can be compared to the reference temperature T_0 as $T_I = T_0 = T_K(1 - k_B/c_v)^{-1}$. The difference of the order $\mathcal{O}(k_B/c_v)$ between T_I and T_K is due to an additional degree of freedom from the fluctuations in internal energy.[40,41] Comparison of the simulation results is shown in Figs. 1(a) and 1(b) for two different time step values. $\Delta t = 0.01\tau$ results in consistent internal and kinetic temperatures, while $\Delta t = 0.05\tau$ leads to values of T_I and T_K which differ by 3%–5%, indicating that this time step is too large. For comparison, the SS algorithm leads to a somewhat smaller temperature difference of 1%–2% for $\Delta t = 0.05\tau$ but shows a relatively strong energy drift. For this test, the SS algorithm implemented in the LAMMPS package[55] has been employed.

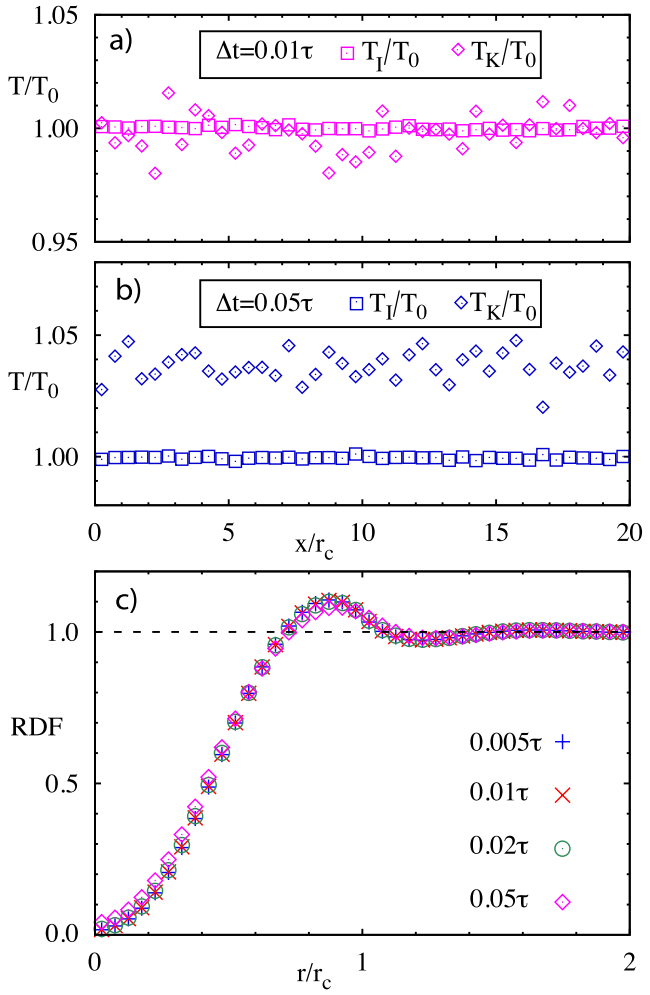

FIG. 1. [(a) and (b)] Comparison of internal T_I/T_0 and kinetic T_K/T_0 temperatures for two different time steps as a function of position within the simulation domain. (c) Radial distribution function (RDF) of fluid particles for various time steps, showing that for $\Delta t \lesssim 0.02\tau$, the RDF is independent of the time step.

Figure 1(a) also shows that the variance of kinetic temperature is markedly higher than that of the internal temperature, which can be rationalized by differences in temperature distributions. The variance of T_K is determined by the Maxwell–Boltzmann distribution of particle velocities and by the number of particles used for T_K averaging.[68] The variance of T_I is given by $\sigma_{T_I}^2 = \sigma_\epsilon^2/c_v^2$, where σ_ϵ^2 is the variance of internal energy, which can be estimated from the distribution of ϵ in the micro-canonical ensemble.[69]

Although we already mentioned that the values of c_v are generally expected to be large, we further probe the limit of the LER algorithm for low c_v values. Our tests show that LER might become unstable for $c_v/k_B < 20$ due the appearance of negative internal energies. In addition, for $c_v/k_B \lesssim 50$, T_K appears to be slightly lower (by 1%–2%) than T_I, while this difference becomes negligible for $c_v/k_B \gtrsim 50$. Therefore, it is recommended to employ the LER algorithm for simulations with $c_v/k_B \gtrsim 50$.

3. Radial distribution function

The measurement of the radial distribution (RDF) function is another test to elucidate the appropriateness of the employed parameters, in particular, the time step. Figure 1(c) demonstrates that $\Delta t \lesssim 0.02\tau$ leads to time step-independent RDF within the fluid. Even though Fig. 1 presents results only for the a^T interaction model, other combinations of the conservative-force coefficient have also been tested, resulting in a similar conclusion. Note that the recommended values of the time step are about one order of magnitude larger than those employed with previous integration methods.[37]

B. Temperature gradients

Different strategies have been employed to simulate thermal gradients,[17,19,70] which can be used in DPDE as well. One of these methods, the velocity exchange algorithm,[19] exactly conserves the overall energy by interchanging the velocity of the fastest particle within a pre-determined cold slab with the slowest particle of a hot slab. Alternatively, the average temperature of two pre-defined layers (or regions) can be set to two unequal values.[71,72] Furthermore, simulations with periodic boundary conditions and temperature gradients often employ hot and cold slabs, in which heat is, respectively, injected and removed, mimicking the contact with reservoirs at different temperatures. In our simulations, heat is injected into the hot slab ($10 < x/r_c < 10.5$) at a constant heat rate of $2J_0A$, where J_0 is the heat flux and $A = L_yL_z$ is the cross-sectional area of the domain, while heat is removed from the cold slab ($0 < x/r_c < 0.5$) at the same rate. Thus, a fixed amount of heat $Q = 2J_0A\Delta t$ is uniformly added or removed every time step from the internal energy of all particles in the volume of a given slab. The factor 2 is due to periodic boundary conditions such that the injected heat Q travels to the left and to the right from the hot slab. Hence, every particle in the hot (cold) slab receives (losses) a heat of Q/N_h (Q/N_c) per time step, where N_h (N_c) is a time-varying number of particles in the hot (cold) slab. In this way, the total energy in the simulation domain is conserved and the temperature gradient can be indirectly regulated by changing the heat rate or flux.

1. Equation of state

First, we test the development of temperature gradient for the three different choices of conservative interactions, using a^T and a^C models with $a_0 = 15k_BT_0/r_c$ and a model with $a_0 = 0$. In the case $a_0 = 0$, the fluid has an ideal-gas equation of state with $p = \rho k_BT$, where p is the pressure and ρ is the density of the fluid. For comparison, isothermal DPD with the a^C model yields an equation of state where pressure varies quadratically in fluid density.[58] The three conservative-force cases are tested for the same linear temperature profile, which is acquired by properly adjusting J_0. Thus, the profile $T(x)/T_0 = 0.018x/r_c + 0.91$ with $T_{min}/T_0 \approx 0.928$ at $x/r_c = 1$ and $T_{max}/T_0 \approx 1.072$ at $x/r_c = 9$ is obtained for the models a^T, a^C, and $a_0 = 0$, with $J_0\tau r_c^2/(k_BT_0) = 2.7$, 2.75, and 2.8, respectively. Figure 2 presents steady-state density profiles for the different models with the same temperature profile, which are nearly linear for all cases. The strongest gradient in fluid density is found for the $a_0 = 0$ model, as expected for a fluid with the ideal-gas equation of state, while the a^C model leads to the least variation in ρ. This means that the a^C model yields a nearly incompressible fluid, while the a^T model shows

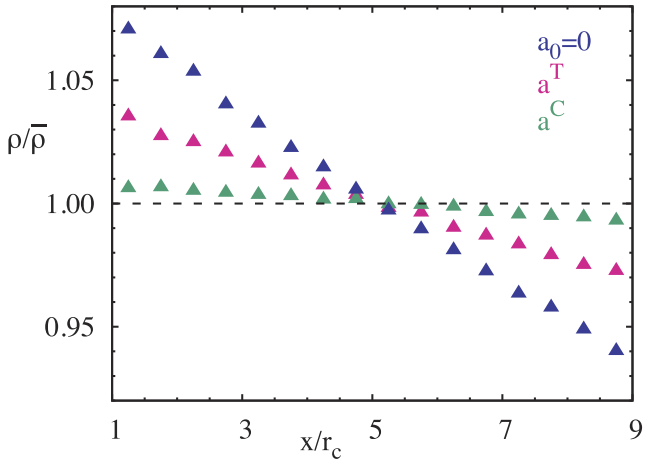

FIG. 2. Steady-state density profiles for three different conservative-force models (see Sec. II D) with the same imposed thermal gradient.

certain compressibility, in qualitative agreement with simple fluids such as water.

2. Heat conductivity

The Fourier law of heat conduction in one dimension,

$$J = \frac{1}{A}\frac{dQ}{dt} = \kappa\frac{dT}{dx}, \tag{10}$$

allows the determination of the thermal conductivity κ in simulations with fixed J_0 by analyzing the resulting temperature gradient. Figure 3 shows three temperature profiles for different J_0. All temperature curves exhibit a nearly linear dependence; however, for the highest J_0 value, the simulation data slightly deviate from the

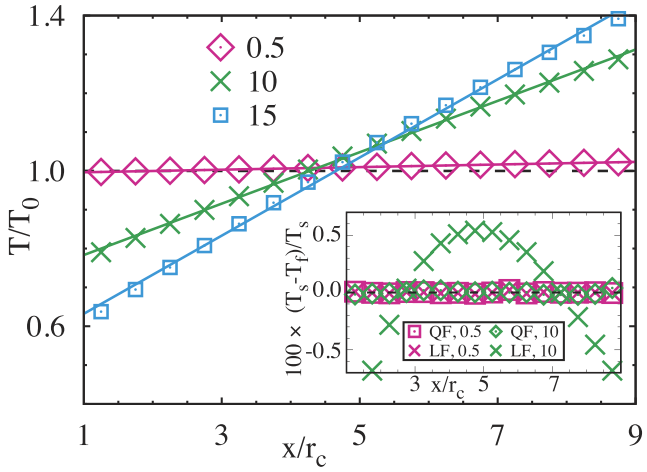

FIG. 3. Temperature profiles for three different $J_0\tau r_c^2/(k_BT_0)$ values. The inset shows deviations of the temperature profile from linear (LF) and quadratic (QF) fits in percents for two different heat flux values.

corresponding linear fit. The deviation of simulated temperature from a linear fit is quantified in the inset of Fig. 3. The temperature profile for $J_0\tau r_c^2/(k_BT_0) = 10$ can be fitted well by a quadratic function. Nevertheless, the deviation of temperature from the linear fit is small and remains within 2%. A large enough heat flux clearly leads to a strong temperature gradient with local changes in fluid density and structure characterized by RDF. This in turn may affect local heat conductivity as it depends on inter-particle distances, resulting in a slightly non-linear temperature profile.

Figure 4(a) presents the dependence of heat conductivity κ on the average fluid temperature and density for the reference parameters, using a small value of $J_0\tau r_c^2/(k_BT_0) = 0.25$. Thermal conductivity increases when average fluid density or temperature increases, which is qualitatively consistent with other experimental and theoretical investigations.[73–76] We will discuss these dependencies in more detail in Sec. III D, where an analytical expression for κ is derived. Figure 4(b) shows the dependence of thermal conductivity κ on heat flux J_0 for different models of conservative interactions. Since κ depends on local temperature and density, it is obtained here by fitting temperature profiles within a small region where particle densities and temperatures are very close to their average values. A temperature-dependent conservative-force coefficient a^T results in slightly smaller heat conductivities in comparison with the constant conservative force with a^C. Heat conductivity exhibits a slight decrease with increasing input heat flux J_0. However, this decrease is within 3%–4%, indicating that κ in the DPDE method is rather robust and nearly independent of the heat flux.

The fact that the DPDE model has a finite value of heat conductivity implies that only a limited amount of heat can be transferred, which determines a maximum heat flux J_{max}. This means that if lager heat fluxes are applied, some parts of the system may attain a negative internal temperature. This is clearly incorrect, as noted already in Ref. 49, and leads to the simulation instability. The maximum heat flux J_{max} depends very strongly on κ_0, especially in the cases where the energy transport by heat conduction dominates over the diffusive transport, and indirectly also on other system parameters, which are more important in cases when the diffusive transport is high (e.g., for low κ_0 values and moderate temperature gradients).

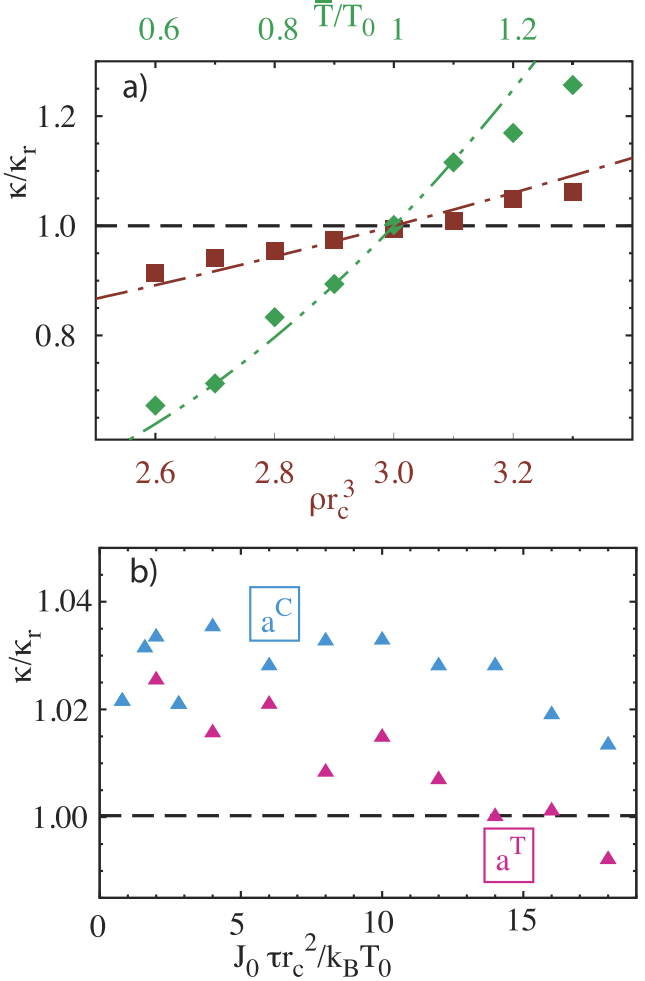

FIG. 4. (a) Normalized heat-conduction coefficient κ/κ_r as a function of temperature and density for relatively weak thermal gradients ($\Delta T/T_0 \lesssim 0.05$). The normalizing factor $\kappa_r = 146\, k_B/(\tau r_c)$ is calculated for the reference values $\bar{\rho} = 3/r_c^3$ and $\bar{T} = T_0$. Dashed dotted lines and the value of κ_r are obtained from the analytical prediction in Eq. (22). (b) Normalized heat-conduction coefficient as a function of the input heat flux for different conservative-force models.

3. Temperature relaxation after sudden localized heating

Another test of the LER algorithm corresponds to a sudden heating of the middle slab $5 < x/r_c < 15$ to the temperature $T/T_0 = 1.5$ (i.e., a 50% temperature increase), followed by temperature relaxation. Figure 5 shows a comparison of the evolution of temperature profiles for the SS and LER algorithms (T_I is shown) and a

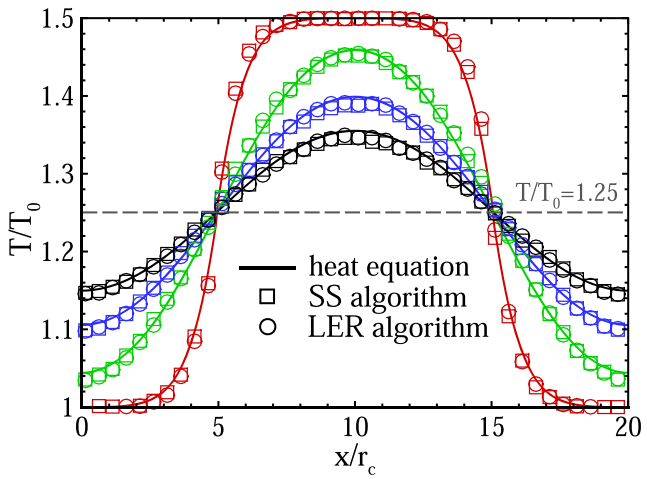

FIG. 5. Evolution of temperature profiles after a sudden heating of the middle slab $5 < x/r_c < 15$ to $T/T_0 = 1.5$ (i.e., a 50% temperature increase) for the SS and LER algorithms (T_I is shown) in comparison with a solution from the heat equation. Each profile is generated from 12 independent simulations, where each point is averaged over 500 time steps. Colors represent averages over the time intervals $[0; 2.5\tau]$—red, $[7.5\tau; 10\tau]$—green, $[15\tau; 17.5\tau]$—blue, and $[22.5\tau; 25\tau]$—black.

solution of the heat equation. Here, we employ a model with a constant conservative coefficient $a^C = a_0$ and $\omega^D = \omega^H = \omega$ with $s = 1$. For the heat equation, fluid conductivity has been set to $\kappa = 300\, k_B/(\tau r_c)$, which was calculated from a simulation of the DPDE fluid under temperature gradient with $\tilde{T}/T_0 = 1.25$. The results in Fig. 5 show an excellent agreement between the two DPDE integration algorithms and the solution of the heat equation, which further supports the validity of the proposed LER algorithm. Note that under extreme local temperature jumps, the two integration algorithms may lead to distinct temperature relaxation behaviors; however, it is not clear whether any of these algorithms give correct results in such cases as there are no reference solutions.

C. Energy transfer

To investigate the mechanisms for heat transfer within a DPDE fluid in more detail, we define a reference plane to monitor the involved energy fluxes. This plane is perpendicular to the gradient direction and can be placed at different positions between the hot and cold slabs. Given a heat flux J_0, energy conservation guarantees that the total energy flux through a plane at any position is constant, $J_{tot} = J_0$. Four different energy fluxes can be distinguished from two different types. One type is a heat-conduction flux, J_C, which corresponds to the exchange of internal energy between fluid particles located at different sides of the plane within distances smaller than the cutoff radius r_c, according to the q^{HC} term in Eq. (7). Another contribution is the diffusive flux J_D of energy, realized by fluid particles which actually cross the plane. Mass conservation enforces that the mass flux through the plane is on average zero, but due to the externally imposed temperature gradient, particles on the hot side are more energetic than on the cold side which results in a diffusive transfer of energy. In this way, diffusive energy transfer includes potential, kinetic, and internal contributions.

Figure 6 shows various contributions to the total energy flux through a plane in the hot area at $x = 8r_c$. The major contributions correspond to the fluxes of particle internal energy, J_C and J^U, while the diffusive fluxes from the potential and kinetic energies, J^P and J^K, are very small. This can be intuitively understood since the ratio between the particle internal energy and potential/kinetic energy is proportional to c_v, which is $c_v/k_B = 200$ here. Note that in this example, the diffusive flux of internal energy J^U is larger than the conductive flux J_C and that $J_{tot} = J_C + J_D$, with $J_D = J^U + J^P + J^K$. Fluctuations of the total flux around the input value are due to the statistical error of the measurement procedure.

Figure 7(a) shows the conductive flux J_C for two conservative-force models through a plane in the hot area at $x/r_c = 8$ as a function of the externally imposed J_0. The conductive flux decays faster for the a^T model in comparison with a^C with increasing J_0. Note that for these two models, the temperature at the reference plane is the same, but the density is different, as can be seen in Fig. 2. This monotonic decay of the conductive flux with increasing J_0 does not occur

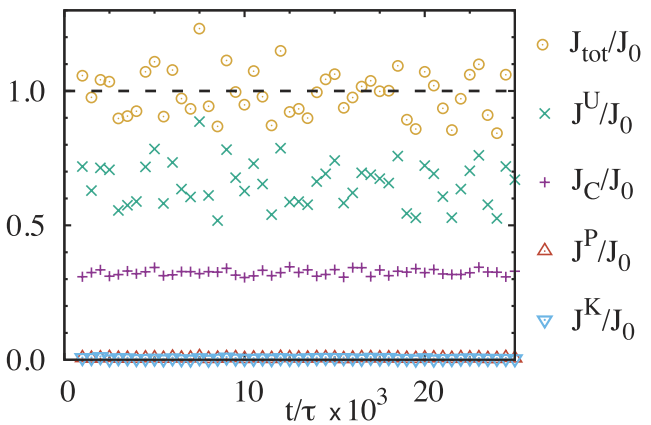

FIG. 6. Energy fluxes through a reference plane at $x = 8r_c$ (hot area) as a function of time: conductive flux of internal energy J_C, and the diffusive fluxes of internal J^U, potential J^P, and kinetic J^K energies. All contributions are normalized by J_0, which is $J_0\tau r_c^2/(k_B T_0) = 6$ here.

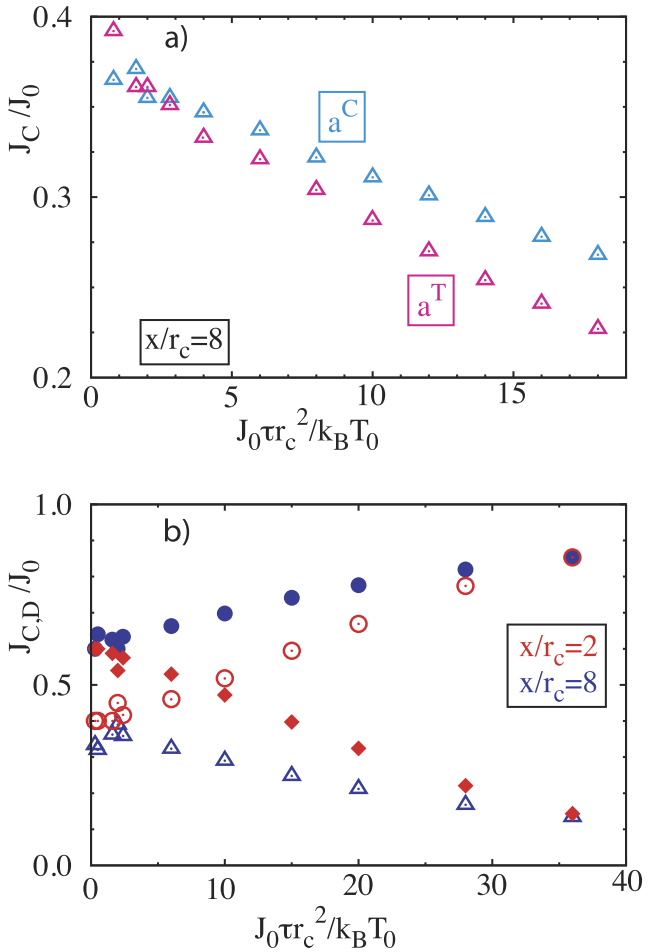

FIG. 7. Energy flux across a plane as a function of the applied J_0. (a) Conductive energy flux at $x/r_c = 8$ for the two types of conservative interactions, a^C and a^T. (b) Conductive (open symbols) and diffusive (solid symbols) contributions to the energy flux measured through a plane in the cold area $x/r_c = 2$ (red) and a plane in the hot area $x/r_c = 8$ (blue). At low temperatures, energy flux is mainly conductive, while at high temperatures, diffusive flux of energy dominates.

though, when the reference plane is placed in the cold area at $x/r_c = 2$, as can be seen by the increase in J_C (open red symbols) in Fig. 7(b). Correspondingly, the diffusive flux J_D increases with the injected heat through the plane at the hot area, while it decreases through the plane at the cold area. Therefore, local temperature strongly affects not only the overall heat conductivity as shown in Fig. 4, but also the ratio between conductive and diffusive fluxes of energy. In Fig. 7(b), this means that on the hot side, the energy flux is mainly diffusive, while on the cold side, it is mainly conductive (for not too small applied heat fluxes).

D. Analytical calculation of energy transfer

In order to provide an analytical expression for the heat-conduction coefficient κ, we analyze both the conductive and diffusive fluxes of the internal energy to total energy transfer since kinetic and potential energies have a much smaller contribution (see Fig. 6). The conductive contribution to the energy transfer between two particles i and j at opposite sides of the reference plane is given by Eq. (7). The random part of heat conduction is zero on average, and the deterministic part can be simplified using the assumption $(T_i + T_j)^2/(T_iT_j) \simeq 4$ which is reasonable for small temperature differences. Then, the average heat rate from Eq. (7) between two particles at the opposite sides of the reference plane becomes

$$q_{C,ij} = \frac{c_v^2}{k_B}\kappa_0(T_j - T_i)\omega^H(r_{ij}). \tag{11}$$

The linear temperature profile can be approximated as $T_j - T_i = \frac{dT}{dx}\Delta x = \frac{dT}{dx}r_{ij}\cos\theta$, where θ is the angle between r_{ij} and the temperature gradient axis (see Fig. 8). Considering that particle j is located at a distance h from the plane, the total heat conduction rate between particle j and its neighbors on the other side of the reference plane is given by

$$q_{C,j}(h) = \rho\int_0^{2\pi}d\phi\int_0^{\theta_c}d\theta\int_h^{r_c}dr_{ij}r_{ij}^2 g(r_{ij})\sin\theta q_{C,ij}, \tag{12}$$

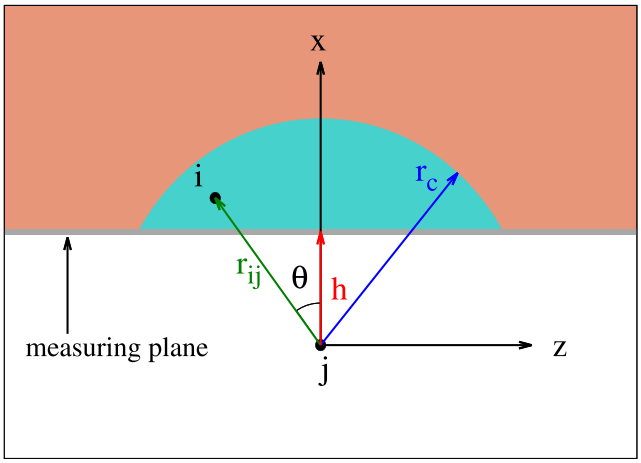

FIG. 8. Heat-conduction integration domain (cyan) for particle j and particle i at opposite sides of the reference plane.

with $\theta_c = \arccos(h/r_c)$. For a non-ideal fluid, the RDF is $g(r_{ij}) \neq 1$ and needs to be pre-computed for the numerical integration of Eq. (12). Total heat rate by conduction is, then, calculated by integrating $q_{C,j}(h)$ over a volume Ar_c as

$$q_C = \rho A\int_0^{r_c} q_{C,j}(h)dh = \frac{\pi\rho^2 c_v^2\kappa_0}{k_B}\frac{dT}{dx}AH(r_c), \tag{13}$$

where A is the area of the reference plane and

$$\begin{aligned} H(r_c) &= \int_0^{r_c}dh\left(1-\frac{h^2}{r_c^2}\right)\int_h^{r_c}drr^3 g(r)\omega^H(r) \\ &= r_c^5\int_0^1 ds(1-s^2)\int_s^1 dll^3 g(lr_c)\omega^H(lr_c) \equiv r_c^5 I_1. \end{aligned} \tag{14}$$

The second equality above makes use of the change in variables $s = h/r_c$ and $l = r/r_c$, while the last equality defines a numerical coefficient I_1, which in general depends on $g(r)$ and $\omega^H(r)$ and, therefore, on the system parameters. With the employed default parameters in Sec. II D, $I_1 = 0.058$.

The second contribution to heat transfer by particle diffusion is calculated by considering particles crossing the reference plane at $x = \text{const}$. It is equal to $q_D^I = N_J\Delta\epsilon$, where N_J is the number of particles crossing the reference plane from hot to cold per unit time. The internal energy transferred by each particle crossing from the hot to the cold side can be calculated as

$$\Delta\epsilon = \bar{\epsilon}(x+\lambda) - \bar{\epsilon}(x-\lambda) \simeq 2\lambda\frac{\partial\bar{\epsilon}}{\partial T}\frac{dT}{dx} = 2\lambda c_v\frac{dT}{dx}. \tag{15}$$

Here, the mean free path λ can be approximated as $\lambda = \tau_c\bar{v}_x$, where τ_c is the collision time and $\bar{v}_x$ is the average velocity of particles crossing the plane in one direction. The collision time is related to the decay of the velocity autocorrelation function, which can be calculated in simulations by assuming an exponential decay of the velocity autocorrelation as

$$\langle\mathbf{v}_i(t)\mathbf{v}_i(0)\rangle = e^{-t/\tau_c}\mathbf{v}_i^2(0). \tag{16}$$

The values of τ_c shown in Fig. 9 have been calculated by fitting an exponential function to direct simulations of the velocity autocorrelation using Eq. (16). In order to provide an analytical estimate for τ_c, we follow the procedure in Ref. 58, where the friction from dissipative interactions defines $1/\tau_c$ and the sum over dissipative forces for neighboring particles is replaced by an integral. The random force vanishes on average and the conservative force determines the RDF such that the expression in Ref. 58 can be generalized to

$$\begin{aligned} \tau_c^{-1} &= \frac{4\pi\gamma\rho}{3m}\int_0^{r_c}drr^2 g(r)\omega^D(r) \\ &= \frac{4\pi\gamma\rho r_c^3}{3m}\int_0^1 dll^2 g(lr_c)\omega^D(lr_c) \equiv \frac{4\pi\gamma\rho r_c^3}{3m}I_2. \end{aligned} \tag{17}$$

The last equality defines the numerical coefficient I_2, which can be calculated for the default parameters in Sec. II D to be $I_2 = 0.131$. Substitution of $\gamma = \sigma^2/(2k_BT)$ (i.e., for $T_i \simeq T_j$) into Eq. (17) results in

$$\tau_c = \frac{3mk_BT}{2\pi\sigma^2\rho r_c^3 I_2}. \tag{18}$$

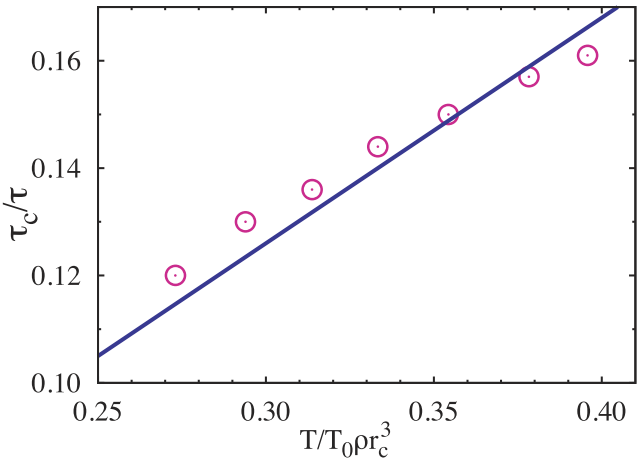

FIG. 9. Collision time calculated for various values of the average temperature and density. Symbols correspond to simulation results, and the solid line corresponds to Eq. (18).

A good agreement between simulated collision times and the analytical approximation is shown in Fig. 9 for different values of the average temperature and density values. Note that the expression in Eq. (17) corresponds to the Vlasov (weak-scattering) approximation[58,77] which might become inaccurate for large fluid viscosities.

Assuming that the mean free path is small, that the temperature gradients are not large, and that the velocity distribution function $f(v)$ can be approximated by the Maxwell–Boltzmann distribution, we can calculate both N_J and $\bar{v}_x$. The number of particles, N_J, crossing the reference plane from hot to cold per unit time, accounts only for particles with positive velocities,

$$N_J = \rho A \int_0^\infty f(v_x) v_x \mathrm{d}v_x = \rho A \sqrt{\frac{k_B T}{2\pi m}}, \tag{19}$$

and the average velocity of those particles is

$$\bar{v}_x = \frac{\int_0^\infty \mathrm{d}v_x v_x f(v_x)}{\int_0^\infty \mathrm{d}v_x f(v_x)} = \sqrt{\frac{\pi k_B T}{2m}}. \tag{20}$$

The results from Eqs. (18)–(20) together yield the diffusive rate of internal energy,

$$q_D^I = \frac{3(k_B T)^2 c_v}{2\pi\sigma^2 r_c^3 I_2} A \frac{\mathrm{d}T}{\mathrm{d}x}. \tag{21}$$

The total heat rate is then the sum of the contributions from Eqs. (13) and (21). With Eq. (10), the heat conductivity can then be approximated as

$$\kappa \simeq \frac{\pi\rho^2 c_v^2 \kappa_0 r_c^5}{k_B} I_1 + \frac{3(k_B T)^2 c_v}{2\pi\sigma^2 r_c^3 I_2}. \tag{22}$$

This analytical expression can be compared with the simulation results shown in Fig. 4, where a very satisfactory agreement is obtained without any adjustable parameters. Note that this quantity has been previously calculated with alternative approaches. The temperature dependence that we obtain in Eq. (22) is similar to that in Ref. 69, where generalized hydrodynamics with a linearized Boltzmann equation was employed. However, the temperature dependence in Eq. (22) is different from that in Ref. 39, where the dissipative contribution was disregarded. The reason for this difference remains to be clarified.

E. Prandtl and Schmidt numbers

A quantitative comparison of the properties of any simulated fluid with those of real fluids can be achieved by considering dimensionless numbers, such as the *Prandtl number*, *Pr*, or the *Schmidt number*, *Sc*. The Prandtl number is the ratio of momentum and energy transport defined as

$$\mathrm{Pr} = \frac{\mu C_P}{\kappa}, \tag{23}$$

where μ and C_P are the dynamic viscosity and specific heat capacity at constant pressure, respectively. For the large values of c_v in DPDE, $C_P \simeq c_v$. The Schmidt number *Sc* is the ratio of momentum and diffusive mass transport defined as

$$\mathrm{Sc} = \frac{\mu}{m\rho D}, \tag{24}$$

where D is the translational diffusion coefficient.

The Prandtl and Schmidt numbers in DPDE are functions of model parameters and can be set to various values independently. The transport properties of a DPD fluid have been investigated in several studies.[56,58,78] Expressions for D and μ have been derived and can be generalized in a similar way as previously shown for the collision time. This yields

$$D = \frac{\tau_c k_B T}{m} = \frac{3(k_B T)^2}{2\pi\sigma^2 \rho r_c^3 I_2}, \tag{25}$$

$$\begin{aligned}\mu &= \frac{\rho D}{2} + \frac{2\pi\gamma\rho^2}{15} \int_0^{r_c} \mathrm{d}r r^4 g(r) \omega^D(r) \\ &= \frac{\rho D}{2} + \frac{\pi\sigma^2\rho^2 r_c^5}{15 k_B T} \int_0^1 \mathrm{d}l l^4 g(l r_c) \omega^D(l r_c) \\ &\equiv \frac{3(k_B T)^2}{4\pi\sigma^2 r_c^3 I_2} + \frac{\pi\sigma^2\rho^2 r_c^5}{15 k_B T} I_3.\end{aligned} \tag{26}$$

Equation (26) defines the numerical coefficient I_3, which can be calculated for the default parameters to be $I_3 = 0.073$, resulting in $Pr = 2.0$ and $Sc = 3.57$. Alternatively, we obtain slightly larger values, $Pr = 2.1$ and $Sc = 4.1$, by keeping all default parameters but considering the ideal case with $g(r) = 1$. Furthermore, different expressions for the weight functions of the conservative, dissipative, and heat terms will lead to different *Pr* and *Sc* values. Liquids have typical *Pr* and *Sc* values within ranges 5–15 and 100–1000, respectively,[79] while for gases, both *Pr* and *Sc* are typically close to unity.[79,80] Thus, our default system lies at the boundary between gaseous and fluid behavior. Using the expressions for transport coefficients above, model parameters (e.g., ρ, r_c, σ, c_v, κ_0) of a DPDE fluid can be selected such that the Prandtl and Schmidt numbers correspond more accurately to those of any given fluid. For example, an increase in the fluid density ρ and/or the cutoff radius r_c will lead to Prandtl and Schmidt numbers which are larger than those employed here but at

the same time will result in an increase in computational cost. Several examples of DPDE simulations in Ref. 37 show that $Sc > 1000$ and $Pr > 10$ are possible to achieve. We have verified that the analytical expressions for Sc and Pr still give a good approximation of these non-dimensional numbers for the examples in Ref. 37, even though these expressions may become less accurate for large fluid viscosities.

IV. SUMMARY AND DISCUSSION

In this paper, various aspects related to the performance of the DPDE method have been systematically investigated. A modification of the velocity-Verlet integration algorithm by local energy redistribution is suggested. In the LER algorithm, the changes in local kinetic and potential energies are exactly counterbalanced by the internal energy every time step at the level of single DPDE particles. This constitutes a simple implementation that leads to approximate conservation of local energy, while the total energy in a simulated system is conserved up to the order of machine precision. The model is validated by verifying the equivalence of the two alternative definitions of the temperature (kinetic and internal), $T_K = T_I$, and by studying the behavior of particle RDF. Although the mesoscopic nature of a DPDE solvent requires that $c_v \gg k_B$, if simulations with $c_v < 50$ are to be considered, it is important to note that the SS-based algorithms have shown to be more stable since negative energies might appear.[41–44] Nevertheless, the main advantage of the LER integration algorithm over a SS scheme is that it is computationally faster and has an easier implementation on parallel computer architectures. These results suggest that the LER algorithm proposed here should be used for studies with $c_v/k_B \gtrsim 50$ and $\Delta t \lesssim 0.02\tau$ (where τ is the unit of time) to guarantee a stable and consistent simulation.

Compressibility effects are especially relevant in the presence of a temperature gradient, due to the related differences in the density distribution, such that we investigate different choices for the conservative interactions. A DPDE fluid with temperature-dependent conservative interactions shows a compressibility lower than a DPDE fluid with an ideal-gas equation of state but clearly larger than a DPDE fluid with constant conservative interactions. Nevertheless, the heat-conduction coefficients are similar for both temperature-dependent and constant conservative interactions.

The interparticle heat-conduction term q^{HC} employed here was originally postulated to be proportional to the particles' inverse-temperature difference, as specified in Eq. (7). Although widely used, this formulation agrees with the Fourier law (and, therefore, with irreversible thermodynamics) only in the limit of small temperature variations. Therefore, an alternative form for the heat-conduction flux, $q_{ij}^{HC} = \widetilde{\kappa}_{ij}\omega^H(r_{ij})(T_j - T_i) + \widetilde{\alpha}_{ij}\zeta_{ij}\left[\omega^H(r_{ij})/\Delta t\right]^{1/2}$ with $\widetilde{\alpha}_{ij}^2 = \widetilde{\kappa}_{ij}T_iT_j$ and $\widetilde{\kappa}_{ij} = c_v\widetilde{\kappa}_0$, has also been proposed.[39,40,81,82] This expression agrees with the Fourier law and satisfies an $\mathcal{H}$-*theorem* and a related fluctuation-dissipation theorem up to the order of $\mathcal{O}(k_B/c_v)$ (see the Appendix of Ref. 81). To fulfill the fluctuation-dissipation theorem exactly, a more sophisticated integration algorithm,[40] which takes possible spurious drifts into account, might be required. Nevertheless, simulations with the q^{HC} formulation above (not shown here) for $c_v/k_B = 200$ using the LER algorithm have displayed no significant differences in comparison with those with the q^{HC} term from Eq. (7), suggesting that the errors are likely small for a large c_v. The correspondence between the two models of q^{HC} was achieved through matching of $\widetilde{\kappa}_0 = \kappa_0 c_v/k_B$, which is a plausible assumption when local temperature differences are not too large (i.e., $T_i \approx T_j$).

The thermal conductivity of the DPDE models is measured in simulations by fitting the Fourier law to an induced temperature gradient. Thermal conductivity describes the system in a very robust manner, showing minor changes for a wide range of temperature gradients. Energy in a DPDE fluid is transferred by the diffusive motion of DPDE particles and by heat conduction due to the internal particle temperature, which depends on local average temperature. The inter-particle conductivity is directly controlled by κ_0, while the diffusive transport depends on the particle friction (or equivalently σ^2) such that depending on local conditions, conductive or diffusive transport of heat may dominate. Good agreement between the analytical expression and simulation measurements of the thermal conductivity is obtained for a large range of parameters. We have also presented analytical approaches to obtain the most important transport coefficients and, therefore, the two most relevant non-dimensional fluid numbers: the Prandtl (Pr) and Schmidt (Sc) numbers. These expressions allow the selection of simulation parameters such that the corresponding Pr and Sc of a DPDE fluid approximate well those of liquids. In conclusion, our results provide a detailed guidance on how to properly employ the DPDE method in simulations of various mesoscopic systems with temperature inhomogeneities.

ACKNOWLEDGMENTS

The authors gratefully acknowledge the computing time granted through JARA-HPC on the supercomputer JURECA[84] at Forschungszentrum Jülich.

APPENDIX: INTEGRATION ALGORITHM WITH LOCAL ENERGY REDISTRIBUTION (LER)

For integration of Eq. (1), the velocity-Verlet algorithm[83] is adapted. In the first integration step, both particle velocities and internal energies are advanced half time step, while particle positions are integrated full time step as follows:

$$\mathbf{v}_i\left(t + \frac{\Delta t}{2}\right) = \mathbf{v}_i(t) + \frac{\mathbf{F}_i(t)}{m_i}\frac{\Delta t}{2}, \tag{A1}$$

$$\epsilon_i\left(t + \frac{\Delta t}{2}\right) = \epsilon_i(t) + q_i(t)\frac{\Delta t}{2} - \left[K_i\left(t + \frac{\Delta t}{2}\right) - K_i(t)\right], \tag{A2}$$

$$\mathbf{r}_i(t + \Delta t) = \mathbf{r}_i(t) + \mathbf{v}_i\left(t + \frac{\Delta t}{2}\right)\Delta t. \tag{A3}$$

Note that the term $[\cdots]$ reflects a change in the particle's kinetic energy $K_i(t) = \frac{m_i}{2}v_i^2(t)$, which is counterbalanced by a portion of internal energy in order to enforce total energy conservation locally. Before the second integration step, particle forces $\mathbf{F}_i(t + \Delta t)$, potential energies $P_i(t + \Delta t)$, and energy rates $q_i(t + \Delta t)$ are computed based on $\mathbf{r}_i(t + \Delta t)$ and $\mathbf{v}_i(t + \Delta t/2)$. In the second step, particle velocities and internal energies are integrated half time step as

$$\mathbf{v}_i(t+\Delta t) = \mathbf{v}_i\left(t+\frac{\Delta t}{2}\right) + \frac{\mathbf{F}_i(t+\Delta t)}{m_i}\frac{\Delta t}{2}, \tag{A4}$$

$$\begin{aligned}\epsilon_i(t+\Delta t) = {} & \epsilon_i\left(t+\frac{\Delta t}{2}\right) + q_i(t+\Delta t)\frac{\Delta t}{2} \\ & - \left[K_i(t+\Delta t) - K_i\left(t+\frac{\Delta t}{2}\right)\right] \\ & - \left[P_i(t+\Delta t) - P_i(t)\right].\end{aligned} \tag{A5}$$

Here, changes in both kinetic and potential energies are offset against the internal energy to satisfy total energy conservation. Potential energy corresponds to the conservative interaction as $\mathbf{F}_{ij}^C = -\vec{\nabla}P_{ij}$ such that $P_i = \sum_j \frac{a_{ij}r_c}{2}\left(1-\frac{r_{ij}}{r_c}\right)^2$.

It is important to note that particle quantities such as $\delta P_i = P_i(t+\Delta t) - P_i(t)$ and $\delta K_i = K_i(t+\Delta t) - K_i(t)$ can only be computed with an accuracy of $\mathcal{O}(\Delta t)$, implying that the local energy is only approximately conserved. Thus, the LER algorithm redistributes the numerically lost or gained energy to exactly restore the energy balance. This energy redistribution is legitimate since it intrinsically follows the original idea of the DPDE method, where the internal energy variable was introduced in order to absorb the imbalance of mechanical energy.[33,34]

REFERENCES

[1] I. V. Pivkin, B. Caswell, and G. E. Karniadakis, in *Reviews in Computational Chemistry*, edited by K. B. Lipkowitz (John Wiley & Sons, Inc., Hoboken, NJ, USA, 2011), vol. 27, pp. 85–110.
[2] R. G. Winkler, D. A. Fedosov, and G. Gompper, Curr. Opin. Colloid Interface Sci. **19**, 594 (2014).
[3] D. A. Fedosov, H. Noguchi, and G. Gompper, Biomech. Model. Mechanobiol. **13**, 239 (2014).
[4] J. Elgeti, R. G. Winkler, and G. Gompper, Rep. Prog. Phys. **78**, 056601 (2015).
[5] U. D. Schiller, T. Krüger, and O. Henrich, Soft Matter **14**, 9 (2018).
[6] G. Gompper, T. Ihle, D. M. Kroll, and R. G. Winkler, Adv. Polym. Sci. **221**, 1 (2009).
[7] G. R. McNamara and G. Zanetti, Phys. Rev. Lett. **61**, 2332 (1988).
[8] X. He and L.-S. Luo, Phys. Rev. E **56**, 6811 (1997).
[9] S. Succi, *The Lattice Boltzmann Equation for Fluid Dynamics and Beyond* (Oxford University Press, Oxford, 2001).
[10] A. Malevanets and R. Kapral, J. Chem. Phys. **110**, 8605 (1999).
[11] A. Malevanets and R. Kapral, J. Chem. Phys. **112**, 7260 (2000).
[12] R. Kapral, Adv. Chem. Phys. **140**, 89 (2008).
[13] P. J. Hoogerbrugge and J. M. V. A. Koelman, Europhys. Lett. **19**, 155 (1992).
[14] P. Español and P. Warren, Europhys. Lett. **30**, 191 (1995).
[15] P. Español and P. B. Warren, J. Chem. Phys. **146**, 150901 (2017).
[16] P. W. Cleary, Appl. Math. Model. **22**, 981 (1998).
[17] S. Sarman and D. J. Evans, Phys. Rev. A **45**, 2370 (1992).
[18] I. Wold and B. Hafskjold, Int. J. Thermophys. **20**, 847 (1999).
[19] D. Reith and F. Müller-Plathe, J. Chem. Phys. **112**, 2436 (2000).
[20] P.-A. Artola, B. Rousseau, and G. Galliero, J. Am. Chem. Soc. **130**, 10963 (2008).
[21] G. Galliero and S. Volz, J. Chem. Phys. **128**, 064505 (2008).
[22] G. Volpe, I. Buttinoni, D. Vogt, H.-J. Kümmerer, and C. Bechinger, Soft Matter **7**, 8810 (2011).
[23] D. A. Fedosov, A. Sengupta, and G. Gompper, Soft Matter **11**, 6703 (2015).
[24] D. Lüsebrink, M. Yang, and M. Ripoll, J. Phys.: Condens. Matter **24**, 284132 (2012).
[25] Z. Tan, M. Yang, and M. Ripoll, Soft Matter **13**, 7283 (2017).
[26] D. P. Sellan, E. S. Landry, J. E. Turney, A. J. H. McGaughey, and C. H. Amon, Phys. Rev. B **81**, 214305 (2010).
[27] G. R. McNamara, A. L. Garcia, and B. J. Alder, J. Stat. Phys. **87**, 1111 (1997).
[28] X. Shan, Phys. Rev. E **55**, 2780 (1997).
[29] M. Yang and M. Ripoll, Phys. Rev. E **84**, 061401 (2011).
[30] M. Yang, R. Liu, M. Ripoll, and K. Chen, Nanoscale **6**, 13550 (2014).
[31] M. Yang and M. Ripoll, Soft Matter **12**, 8564 (2016).
[32] M. Langenberg and M. Müller, Europhys. Lett. **114**, 20001 (2016).
[33] P. Español, Europhys. Lett. **40**, 631 (1997).
[34] J. Bonet Avalos and A. D. Mackie, Europhys. Lett. **40**, 141 (1997).
[35] E. Abu-Nada, Phys. Rev. E **81**, 056704 (2010).
[36] T. Yamada, A. Kumar, Y. Asako, O. J. Gregory, and M. Faghri, Numer. Heat Transfer, Part A **60**, 651 (2011).
[37] Z. Li, Y.-H. Tang, H. Lei, B. Caswell, and G. E. Karniadakis, J. Comput. Phys. **265**, 113 (2014).
[38] T. Yamada, E. O. Johansson, B. Sundén, and J. Yuan, Numer. Heat Transfer, Part A **70**, 595 (2016).
[39] J. Bonet Avalos and A. D. Mackie, J. Chem. Phys. **111**, 5267 (1999).
[40] A. D. Mackie, J. Bonet Avalos, and V. Navas, Phys. Chem. Chem. Phys. **1**, 2039 (1999).
[41] M. Lísal, J. K. Brennan, and J. Bonet Avalos, J. Chem. Phys. **135**, 204105 (2011).
[42] A.-A. Homman, J.-B. Maillet, J. Roussel, and G. Stoltz, J. Chem. Phys. **144**, 024112 (2016).
[43] J. P. Larentzos, J. K. Brennan, J. D. Moore, M. Lísal, and W. D. Mattson, Comput. Phys. Commun. **185**, 1987 (2014).
[44] G. Stoltz, J. Comput. Phys. **340**, 451 (2017).
[45] G. Faure and G. Stoltz, Appl. Math. Mech. **39**, 83 (2018).
[46] M. Lísal, J. P. Larentzos, M. S. Sellers, I. V. Schweigert, and J. K. Brennan, J. Chem. Phys. **151**, 114112 (2019).
[47] C. A. Marsh, G. Backx, and M. H. Ernst, Europhys. Lett. **38**, 411 (1997).
[48] S. R. de Groot and P. Mazur, *Non-Equilibrium Thermodynamics* (North-Holland, Amsterdam, 1962).
[49] M. Ripoll, P. Español, and M. H. Ernst, Int. J. Mod. Phys. C **9**, 1329 (1998).
[50] R. Qiao and P. He, Mol. Simul. **33**, 677 (2007).
[51] C. A. Marsh and P. V. Coveney, J. Phys. A: Math. Gen. **31**, 6561 (1998).
[52] T. Shardlow, SIAM J. Sci. Comput. **24**, 1267 (2003).
[53] G. De Fabritiis, M. Serrano, P. Español, and P. V. Coveney, Physica A **361**, 429 (2006).
[54] M. Serrano, G. De Fabritiis, P. Español, and P. V. Coveney, Math. Comput. Simul. **72**, 190 (2006).
[55] S. Plimpton, J. Chem. Phys. **117**, 1 (1995).
[56] X. Fan, N. Phan-Thien, S. Chen, X. Wu, and T. Y. Ng, Phys. Fluids **18**, 063102 (2006).
[57] D. A. Fedosov, I. V. Pivkin, and G. E. Karniadakis, J. Comput. Phys. **227**, 2540 (2008).
[58] R. D. Groot and P. B. Warren, J. Chem. Phys. **107**, 4423 (1997).
[59] I. Pagonabarraga and D. Frenkel, J. Chem. Phys. **115**, 5015 (2001).
[60] P. B. Warren, Phys. Rev. Lett. **87**, 225702 (2001).
[61] P. B. Warren, Phys. Rev. E **87**, 045303 (2013).
[62] P. Nikunen, M. Karttunen, and I. Vattulainen, Comput. Phys. Commun. **153**, 407 (2003).
[63] F. Thalmanna and J. Farago, J. Chem. Phys. **127**, 124109 (2007).
[64] S. Litvinov, M. Ellero, X. Y. Hu, and N. A. Adams, J. Comput. Phys. **229**, 5457 (2010).
[65] B. Leimkuhler and X. Shang, J. Comput. Phys. **280**, 72 (2015).
[66] T. Yamada, S. Itoh, Y. Morinishi, and S. Tamano, J. Chem. Phys. **148**, 224101 (2018).
[67] P. Español, M. Serrano, I. Pagonabarraga, and I. Zúñiga, Soft Matter **12**, 4821 (2016).
[68] R. López-Ruiz and X. Calbet, Am. J. Phys. **75**, 752 (2007).
[69] M. Ripoll, Ph.D. thesis, UNED, Spain, 2002.
[70] D. Lüsebrink and M. Ripoll, J. Chem. Phys. **136**, 084106 (2012).
[71] C. M. Pooley and J. M. Yeomans, J. Phys. Chem. B **109**, 6505 (2005).

[72]M. Yang and M. Ripoll, Soft Matter **9**, 4661 (2013).
[73]S. Chapman, T. G. Cowling, and D. Burnett, *The Mathematical Theory of Non-uniform Gases* (Cambridge University Press, Cambridge, 1990).
[74]L. A. Guildner, J. Res. Natl. Bur. Stand., Sect. A **79**, 407 (1975).
[75]H. J. M. Hanley, R. D. McCarty, and W. M. Haynes, J. Phys. Chem. Ref. Data **3**, 979 (1974).
[76]H. Ziebland and J. T. A. Burton, Br. J. Appl. Phys. **6**, 416 (1955).
[77]A. J. Masters and P. B. Warren, Europhys. Lett. **48**, 1 (1999).
[78]H. Noguchi and G. Gompper, Phys. Rev. E **78**, 016706 (2008).
[79]D. R. Lide, *CRC Handbook of Chemistry and Physics* (CRC Press, Boca Raton, FL, 2004).
[80]J. Kestin, K. Knierim, E. A. Mason, B. Najafi, S. T. Ro, and M. Waldman, J. Phys. Chem. Ref. Data **13**, 229 (1984).
[81]M. Ripoll and M. H. Ernst, Phys. Rev. E **71**, 041104 (2005).
[82]M. Ripoll and M. H. Ernst, Phys. Rev. E **72**, 011101 (2005).
[83]M. P. Allen and D. J. Tildesley, *Computer Simulation of Liquids* (Clarendon Press, New York, 1991).
[84]Jülich Supercomputing Centre, J. Large-Scale Res. Facil. **4**, A132 (2018).